CHEMISTRY OF MATERIALS

Article

pubs.acs.org/cm

Low Temperature Epitaxial Oxide Ultrathin Films and Nanostructures by Atomic Layer Deposition

Mariona Coll,[†,*] Jaume Gazquez,[†,‡] Anna Palau,[†] Maria Varela,[‡,§] Xavier Obradors,[†] and Teresa Puig[†]

[†]Institut de Ciencia de Materials de Barcelona (ICMAB-CSIC), Campus UAB, 08193 Bellaterra, Spain

[‡]Materials Science and Technology Division, Oak Ridge National Laboratory, Oak Ridge, Tennessee 32831, United States

[§]Departamento de Física Aplicada III, Universidad Complutense de Madrid Madrid 28040, Spain

Supporting Information

ABSTRACT: Highly epitaxial and pure (001) CeO_2 ultrathin films have been prepared by atomic layer deposition (ALD) at 275 °C on Y-stabilized ZrO_2 cubic fluorite single crystal substrate using cerium β-diketonate ($Ce(thd)_4$) and ozone (O_3) as precursors. Substrate temperature and precursor pulses have been optimized to set the ALD window obtaining a growth per cycle of ≈0.2 Å/cycle. This extremely low growth rate has been identified as a key parameter to ensure epitaxial growth at these low temperatures. Post-thermal treatments at 900 °C in oxygen further improve ALD-CeO_2 film texture while maintaining film stoichiometry and ultrasmooth surface, rms < 0.4 nm. ALD-CeO_2 thin film growth has also been tested on perovskite single crystal substrates, $SrTiO_3$ and $LaAlO_3$, exhibiting CeO_2 epitaxial growth and thus validating ALD as an outstanding method for low temperature epitaxial growth. Furthermore, we demonstrate that by combining e-beam lithography and ALD it is feasible to obtain size-controlled CeO_2 nanostructures.

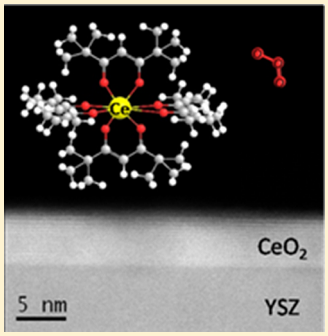

KEYWORDS: *atomic layer deposition, epitaxial film, CeO_2, low temperature growth, area-selective atomic layer deposition*

INTRODUCTION

CeO_2 is a very attractive material widely known for its use in catalysis,[1] energy storage systems,[2] gas sensing,[3] ultraviolet filtration,[4] and polishing agent.[5] Epitaxial growth of CeO_2 thin films has generated huge interest for silicon-on-insulator structures[6,7] and also as buffer layer in functional oxide heterostructures such as high temperature superconductors (HTS) coated conductors and microelectronic devices.[8−10] For most of these applications, slight changes in film thickness, composition, degree of epitaxy, or the presence of defects can dramatically affect the system properties. Preparation of epitaxial (doped)-CeO_2 films has been achieved by several physical[7,11,12] and chemical deposition techniques.[13,14] In particular, atomic layer deposition (ALD)[15] is a unique chemical gas-phase deposition technique where the film growth proceeds through self-limiting surface reaction achieved through alternate pulsing of the precursors.[16,17] This ensures excellent large-area uniformity and conformity and enables simple and atomic layer control of film thickness and composition. Also, ALD can be performed at lower deposition temperatures than other vacuum deposition techniques such as PLD or CVD, which guarantees low thermal budget, low interdiffusion, and the possibility to use organic or biological substrates. However, little work has been reported on ALD epitaxial growth,[18−20] since ALD has been mostly devoted to grow high dielectric insulators on semiconductors and 3D substrates (aerogels, porous alumina), which usually lead to amorphous or polycrystalline films.[21−23] Similarly, ALD-CeO_2 has only been investigated on silicon-based substrates, resulting in polycrystalline films.[24−26] The use of single crystal substrates with similar crystal structure and/or similar lattice parameters with the film may promote epitaxial growth,[27] but a comprehensive study of epitaxial ALD-CeO_2 growth is still lacking. Here, we tackle this challenge. For CeO_2, which has a cubic fluorite structure, fluorite (100) Y-stabilized ZrO_2 with lattice misfit (ε) of −4.8%[14,28] or perovskite (100)$SrTiO_3$ (ε = 1.7%) and (100)$LaAlO_3$ (ε = −1.2%)[29−31] are potentially attractive substrates, not only from a fundamental standpoint of surface science[32−35] but also because they can simultaneously facilitate the integration of ferroelectric and colossal magnetoresistive materials in microelectronics[36] and oxide electronics[37] and the fabrication of superconducting coated conductors.[8,38]

The self-limiting surface reaction ALD characteristics make the interaction between metalorganic precursors and surface reactive sites on the film deposition crucial. Controlling such interaction provides an opportunity to nanoengineer the surface properties and control the thin film growth in designated areas and in 3D nanostructures to create new functionalities.[21] This makes ALD a very attractive approach to fabricate CeO_2 nanostructures, their properties being strongly dependent on their morphology, size, and orientation.[39−41] The use of self-assembled monolayers (SAMs) with different functional end groups and polymer films (polymethyl metacrylate, PMMA) is an effective route to modify the surface

Received: June 15, 2012
Revised: August 23, 2012
Published: September 4, 2012

properties of the substrate and thus activate or inhibit the chemisorption sites for ALD precursors, especially when water is used as an oxidizing agent.[42−47] However, more aggressive oxidant atmospheres such as ozone[48] and moderate deposition temperatures[49] can degrade the organic layers and frustrate the area-selective ALD process. Alternatively, electron-beam and soft-lithography techniques have been recently explored to create activated areas for the selective deposition of ALD metals.[50,51] In this work we report the preparation of low temperature, 275 °C, and highly epitaxial as-deposited ALD-CeO_2 ultrathin films on various single crystal substrates (fluorite (YSZ) and perovskite (STO, LAO) structures) using cerium β-diketonates ($Ce(thd)_4$) and ozone (O_3) as reactive precursors. Post-thermal treatments at 700, 800, and 900 °C have been performed to study further improvement of film crystallinity. Also, we demonstrate that ALD-CeO_2 nanostructures (with lateral dimension from 600 nm to 2 μm) can be obtained combining PMMA resist layer and e-beam lithography even when the ALD process uses O_3 as oxidant reactant. X-ray diffraction (XRD), X-ray photoelectron spectroscopy (XPS), atomic force microscopy (AFM), reflection high energy electron diffraction (RHEED), and scanning transmission electron microscopy (STEM) confirmed the formation of ultrasmooth, pure, relaxed, and epitaxial (00l) CeO_2 films.

EXPERIMENTAL SECTION

ALD of CeO_2 Films. CeO_2 films were prepared in a Cambridge Nanotech Savannah 200 flow-type ALD reactor using commercial $Ce(thd)_4$ (thd = tetrakis(2,2,6,6-tetramethyl-3,5-heptanedionato) (STREM) and ozone (O_3) as the oxygen source on 5 × 5 mm^2 (100) yttria-stabilized ZrO_2 (YSZ), (100) $SrTiO_3$ (STO), and (100) $LaAlO_3$ (LAO) substrates. Single crystal substrates were cleaned by 5 min of sonication in ethanol and dry N_2. ALD CeO_2 deposition was optimized on YSZ substrates studying the precursor sublimation temperature (160−180 °C), substrate temperature (150−300 °C), and Ce pulse times; see Supporting Information. The low volatility of cerium β-diketonate compound ($Ce(thd)_4$)[52] required pseudoboost conditions to guarantee the sublimation and delivery of the precursor into the reaction chamber. Substrate temperature range of 200−275 °C was identified with constant growth rates indicating the presence of a true ALD temperature window. Pulse and purge times for $Ce(thd)_4$ varied from 0.25 to 4 s and 2−20 s, respectively, and pulse and purge times for O_3 were set at 2.5 and 15 s.[25] High purity N_2 (99.9995%) was used as carrier and purge gas with a gas flow of 20−50 sccm. Films were deposited using 200−900 cycles.

Patterned ALD CeO_2. CeO_2 nanostructures have been prepared using YSZ substrates decorated with silver patterns performed by e-beam lithography (EBL). A YSZ substrate was spin-coated with MMA/PMMA 950K resist bilayer to give a 200 nm thick film. Both layers were baked on a hot plate for 1 min at 180 °C. Several arrays of nanostructures were generated with EBL using exposures with 10 KeV beam energy, 105 pA beam current, and area doses of 50−70 $\mu As/cm^2$. After resist development, a 30 nm Ag layer was thermally evaporated followed by a MMA/PMMA lift-off in hot acetone. CeO_2 was deposited on Ag decorated substrate from $Ce(thd)_4$ and O_3 at 200 °C for 150 cycles. Finally, Ag etching was performed in 5% HNO_3 aqueous solution resulting in the desired CeO_2 nanostructures.

CeO_2 Characterization. Film purity, crystallinity and thickness were studied using Rigaku Rotaflex RU-200BV X-ray diffractometer with Cu Kα λ = 1.5418 Å. Texture analysis was perfomed using a XRD^2 GADDS D8 Advance system from Bruker. Surface morphology was evaluated by atomic force microscopy with a microscope 5500 from Agilent Technologies. Surface crystallinity was evaluated by RHEED measurements, monitored in a STRAIB Instrument, using a 30 kV electron gun under high pressure, 2 × 10^{-8} mbar, at room temperature at different incident angles (0.5−3°). The software used for observation is KSA400 (K-Space). Surface chemical composition of CeO_2 films was studied by Kratos Axis Ultra X-ray Photoelectron Spectroscopy with Al Kα source (1486 KeV), pass energy of 160 eV for survey spectra and 20 eV for high resolution spectra, at Instituto de Nanociencia de Aragon (INA), Zaragoza, Spain. To compensate charging effects, all spectra were calibrated with respect to the C(1s) peak at 284.6 eV. Scanning transmission electron microscopy (STEM) images have been acquired using a Nion UltraSTEM operated at 100 kV and equipped with a NION aberration corrector at Oak Ridge National Laboratory (ORNL), Oak Ridge, TN, USA. TEM specimens were thinned by mechanical grinding, polishing, and dimpling, followed by Ar-ion milling. E-beam lithography was performed by a field emission scanning electron microscope (SEM) QUANTA FEI 200 FEG-ESEM.

Thermal treatments of as-deposited ALD films were carried out in an Annealsys rapid thermal annealing furnace (RTA) As-Micro at 700−900 °C for 15 min under oxygen atmosphere with a 20 °C/s heating ramp.

RESULTS AND DISCUSSION

Film crystallinity and phase purity of ALD-CeO_2 films on YSZ single crystal substrates were investigated from X-ray diffraction $\theta-2\theta$ scans of as-deposited film at 275 °C and post-annealed films at 700, 800, and 900 °C under oxygen atmosphere, as shown in Figure 1a. Subtle shoulders at 2θ = 33° and 69° can

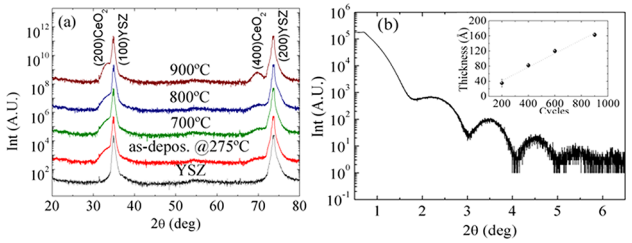

Figure 1. (a) X-ray diffraction $\theta-2\theta$ scans of 200 cycles of ALD-CeO_2 on YSZ single crystal deposited at 275 °C and post-annealed at 700, 800 and 900 °C under oxygen atmosphere. (b) X-ray reflectometry from as-deposited 400 cycles ALD-CeO_2 film. Inset shows thickness dependence on the number of cycles for as-deposited ALD films.

be identified in as-deposited CeO_2 films compared to YSZ bare substrate, revealing epitaxial (00l) CeO_2 growth. $\theta-2\theta$ scans of thermal treated films up to 800 °C do not show any significant change in film crystallinity. By increasing the annealing temperature up to 900 °C, the integrated intensity of (00l)CeO_2 reflections is largely enhanced, which is attributed to an increase of film crystallinity. In-plane (ϕ scan CeO_2(111)) and out-of plane (ω-scan CeO_2(200)) grain orientation measurements have been acquired from as-deposited and post-treated films. The as-deposited films showed $\Delta\phi$ = 1.1° and $\Delta\omega$ = 0.9°, whereas post-treated films at 900 °C showed $\Delta\phi$ = 0.8° and $\Delta\omega$ = 0.6°. The decrease in both values in the post-treated film confirms film texture improvement after post-treatment. The quality of the ALD-CeO_2 film crystallinity is comparable to the quality obtained by other chemical[53,54] and physical deposition techniques[12] on YSZ.

X-ray reflectometry (XRR) of films deposited in a range of 200−900 cycles was monitored to control as-deposited film thickness dependence; see Figure 1b. The linear dependence supports surface-limiting reaction with a growth per cycle of 0.2 Å/cycle. This growth rate entails less than 5% of a monolayer per cycle, and it is substantially low, as expected from the large size and molecular weight of the thd precursors.[25,55−57] Faster growth rates were obtained in ALD-CeO_2 when using

dx.doi.org/10.1021/cm301864c | Chem. Mater. 2012, 24, 3732−3737

cyclopentadienil (Cp) and N-based metalorganic precursors; however, these precursors do not add any improvements in terms of film quality (polycrystalline films) with respect to thd's.[25,26] $Ce(thd)_4$ molecules can be adsorbed on YSZ substrate by ligand exchange, dissociation, or association; see Figure 2. However, the reaction mechanism for this system is

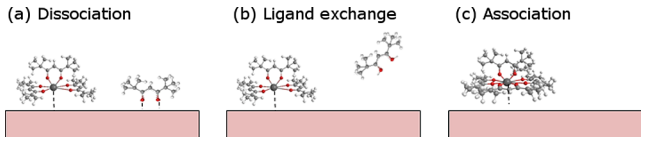

Figure 2. Schematic of the possible adsorption mechanisms for the $Ce(thd)_4$ complex on a surface. (a) Dissociation: Ce precursor releases a thd ligand when adsorbed on the substrate and the ligand attaches to the surface substrate as well. (b) Ligand exchange: Ce precursor releases a thd ligand when adsorbed and the thd is eliminated as a reaction product. (c) Association: Ce precursor adsorbs on the substrate with no release of thd ligands. Large gray spheres represent Ce^{4+}, red spheres represent O atoms, small gray spheres represent C, and white spheres represent H atoms.

barely investigated.[58] By applying the theoretical model based on the mass balance of chemisorption described by Puurunen,[57] the chemisorption mechanism for a particular ALD system can be estimated. For our system, in the linear regime, it is likely that ligand exchange reaction occurs, that is, release of organic ligands when cerium chemisorbs to the YSZ surface as the calculated experimental concentration of Ce per monolayer, 0.58 nm^{-2}, is higher than the theoretical value when assuming no thd is released upon adsorption, 0.25 nm^{-2}. A similar chemisorption mechanism has been previously described by the $Y(thd)_3$ and O_3 process on Si.[59] Nonetheless, the identification of the elementary chemical reactions that take place during the $Ce(thd)_3/O_3$ pulse deposition and the associated activation energies would be required to fully elucidate the reaction mechanism for this CeO_2/YSZ system.

Surface morphology and surface crystallinity were evaluated by AFM and RHEED, respectively. Figure 3a,b shows the AFM

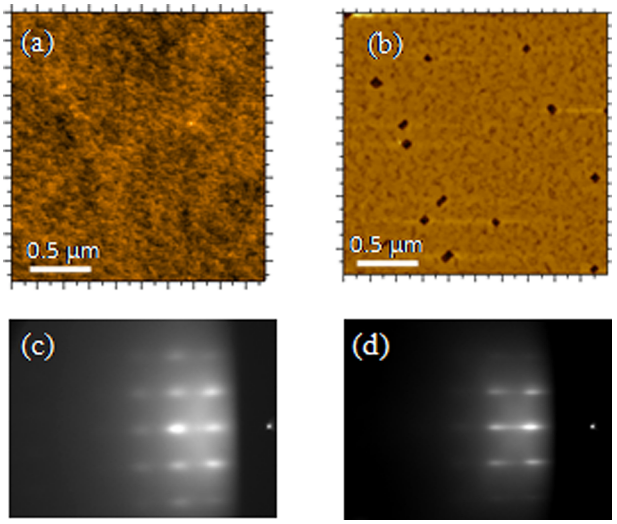

Figure 3. AFM of (a) as-deposited and (b) annealed at 900 °C of 200 cycles ALD CeO_2 thin films. RHHED patterns acquired along the ⟨100⟩ YSZ substrate direction in (c) as-deposited and (d) annealed at 900 °C ALD CeO_2 films.

topographic images of as-deposited and post-annealed at 900 °C CeO_2 film, respectively. In both cases, homogeneous ceria films with an rms ≤ 0.4 nm are observed. This atomically flat surface is consistent with the self-limiting surface reaction of ALD. The square-shaped features observed in the post-treated sample, Figure 3b, are attributed to film dewetting. The cavity size can vary from 10 nm up to 70 nm within the sample (see Supporting Information). This film instability has been previously observed in heteroepitaxial growth of $YBa_2Cu_3O_7$ films, and it has been identified as a mechanism to relieve the stress induced at the interface by the lattice misfit between the layer and the substrate in very thin films at high processing temperatures,[60] in accordance with the present results. It is important to note that thicker films and shorter processing times can overcome dewetting in ALD-CeO_2 films while keeping high crystalline quality; see Supporting Information.

From the RHEED diffraction patterns acquired in the ⟨100⟩ direction of YSZ single crystal substrate with a grazing angle (α_1) of 1.5°, ordered streaks along the crystal direction (00*l*) are identified in both films (c) as-deposited and (d) annealed at 900 °C, confirming (001) epitaxiality up to the CeO_2 film surface. The appearance of streaks also supports the formation of atomically flat surfaces as anticipated by AFM.

The chemical composition of ALD ceria films was evaluated by XPS analysis. The survey spectrum presented in Figure 4a

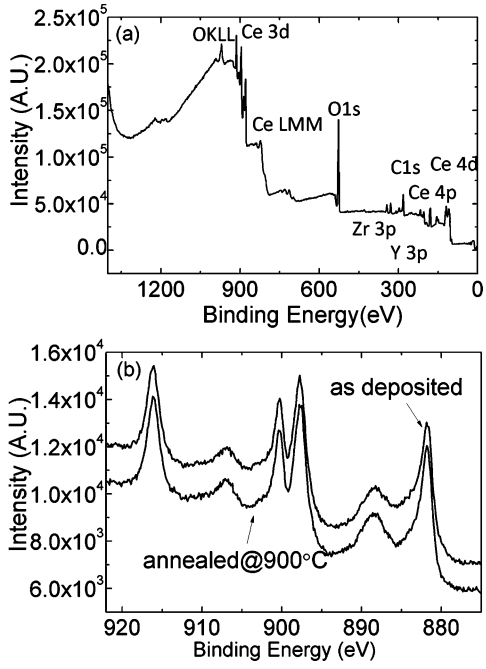

Figure 4. XPS (a) survey and (b) high resolution Ce(3d) spectra of as-deposited and annealed 200 cycles of ALD CeO_2 films on YSZ single crystal substrate.

shows the existence of Ce, O, C, Y, and Zr consistent with the presence of ceria and YSZ substrate. The detection of Y and Zr is explained by the very thin CeO_2 thickness when deposited 200 cycles. The C contribution is attributed to atmospheric contamination since this peak is strongly reduced after 2 min sputtering with Ar^+. It is likely that the low growth per cycle identified in this process can help eliminate the C contamination throughout the film thickness. The high resolution XPS Ce(3d) region of both as-deposited and annealed at 900 °C ALD CeO_2 films is shown in Figure 4b.

dx.doi.org/10.1021/cm301864c | *Chem. Mater.* 2012, 24, 3732−3737

The Ce(3d) spectral region is rather complex, showing three spin orbit doublets appearing at 881.9 eV (v), 888.4 eV (v″), 897.8 eV (v‴), 900.2 eV (u), 907.3 eV (u″), and 916.0 eV (u‴), all of them attributed to the presence of Ce^{4+} and in good agreement with reference data.[61,62] Minimal changes in the Ce(3d) region spectra between as-deposited and annealed at 900 °C films indicate that both films are stoichiometric CeO_2.

Atomic-resolution STEM analysis of as-grown and post-annealed CeO_2 samples reveal that epitaxial CeO_2 films have indeed grown at 275 °C on the (001) YSZ substrate; see Figure 5. The as-deposited CeO_2 film is continuous over long lateral

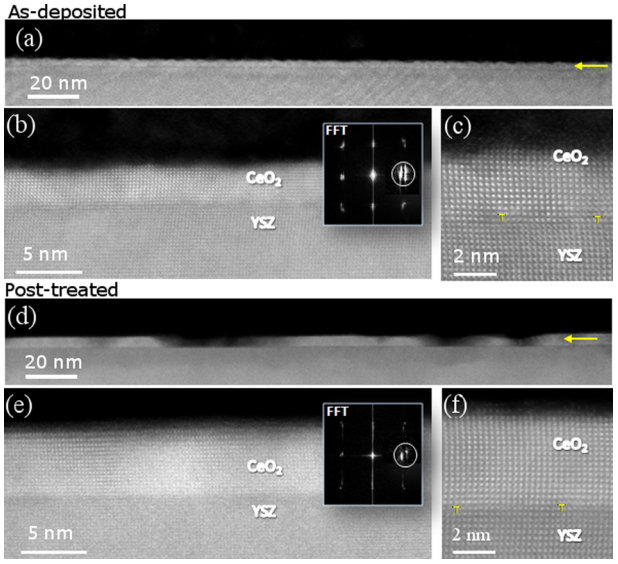

Figure 5. ADF-STEM images of 200 cycles ALD-CeO_2 films grown on YSZ substrate and viewed along the CeO_2[100]/YSZ[100] zone axis. (a, b and d, e) Low and high magnification ADF Z-contrast images of as-deposited and post-treated CeO_2 films, respectively. Insets show the corresponding FFT patterns. Arrows point to the CeO_2 layer. (c and d) High magnification Z-contrast images of the interface between ceria and the substrate of as-deposited and post-treated CeO_2 films, respectively. ALD CeO_2 films were post-treated at 900 °C, 15 min in oxygen. Arrows mark the position of misfit dislocations.

distances, (figure 5 (a)), whereas the post-treated film shows bare-substrate regions, figure 5 (d), as previously identified by AFM. High magnification ADF Z-contrast images of both samples and their corresponding fast Fourier transform (FFT) patterns confirm a cube on cube epitaxial relationship between the whole film and the substrate for both as-grown and post-annealed samples. The splitting of the film and substrate diffraction spots in FFT, those closer to the center belonging to the ceria, is also consistent with a fully relaxed film, which is confirmed by the presence of misfit dislocations at the substrate interface; see Figure 5c,f. The presence of a high amount of misfit dislocations can be attributed to the exceptionally low deposition rate of this ALD-CeO_2 system. The film thickness of as-deposited 200 cycles ALD-CeO_2 films is ≈3 nm, which corresponds to six CeO_2 unit cells; see Figure 5b and is consistent with XRR data. After a post-thermal treatment, the same film shows an apparent film thickness of 5 nm, Figure 5e, as a consequence of the isolated dewetted regions preserving the film volume.

We observe that in ALD, in contrast to other deposition methods, epitaxy can be achieved at very low deposition temperatures (250−300 °C) with no need of ultra-high vacuum. In vacuum deposition techniques, deposition rate (R) and substrate temperature (T) have been identified as key parameters to control the thin film growth process.[27] These two terms can be used to determine the activation energy for an adatom to be stable or unstable on a substrate surface, E_{des}.[63] The number of atom bonds available in the substrate surface will also influence E_{des}, particularly in ALD deposition as it depends on self-saturating surface reactions. When the vapor precursor impinges on the substrate it usually remains on the surface for a period of time, τ, and the atoms are capable of diffusing a certain distance. At high temperature, diffusion, D, is usually very fast and does not limit nucleation.[64] At low temperature, lower values of the diffusion coefficient, that is, large adatom average migration time to the equilibrium sites, changes the nucleation scenario, and monomer density, n_1, may play an important role.[65] The formation of crystalline deposits depends on the surface density of the adatoms (n) and on the surface-diffusion-incorporation time of the adatoms, τ. Since τ is thermally activated, low deposition temperatures and the use of a lattice mismatched substrate may yield good epitaxy.[27]

In this case, a sequential deposition technique such as ALD could help control the monomer distribution and therefore the final density of epitaxial clusters. Therefore, it is likely that the extremely low growth rates (low temperature deposition) identified for CeO_2-ALD films, ≈ 0.016 nm/min along with the use of YSZ single crystal substrate, facilitates the epitaxial orientation of ceria films. Epitaxial CeO_2 thin films (>10 nm) on single crystal substrates deposited by vacuum techniques, CVD,[66] MBE,[31,67] and PLD,[29,30,68] are achieved at T > 550 °C and R ranging from 0.1 nm/min to 200 nm/min. Clearly, faster deposition rates need higher temperatures to guarantee epitaxial growth. Chemical solution methodologies, where all of the precursor is already on the substrate surface at the beginning of the thermal process, allow epitaxial CeO_2 by island growth mode at T > 800 °C.[14,33]

To demonstrate the viability of low temperature ALD-CeO_2 epitaxial growth we tested the growth on dissimilar crystalline heterostructures where interface energy could play a larger role in impeding 2D growth. We prepared ALD-CeO_2 films on single crystal substrates with cubic perovskite structure such as (100)STO and (100)LAO substrates which are particularly interesting because they have a small difference in lattice parameters, ε_{STO} = 1.7% and ε_{LAO} = −1.2%, as ceria grows epitaxially rotated 45° in the plane axis to the substrate.[30] Also, fluorite/perovskite systems are attractive for solid oxide fuel cells applications,[69] and strained interfaces display several orders of magnitude increase of ionic conductivity.[70] To compare, YSZ exhibits a cubic fluorite structure, as CeO_2, and has a lattice misfit of ε = −4.8%, with cube on cube epitaxial growth. Figure 6 shows X-ray diffraction θ−2θ scans of the ALD-CeO_2 films deposited on (100)YSZ, (100)STO, and (100)LAO. In all cases (00l) CeO_2 reflections are observed; however, significant differences in CeO_2 peak shape and intensity can be easily identified. The in plane texture of ALD-CeO_2 on (100)STO is $\Delta\phi$ = 1.9° and on (100)LAO is $\Delta\phi$ = 4°. Out-of-plane measurements show values of $\Delta\omega$ = 1.5° on (100)STO and $\Delta\omega$ = 0.3° on (100)LAO. These variations are tentatively attributed to different film thickness and crystalline quality as the operating ALD conditions were optimized for YSZ and it is expected that a different substrate surface chemistry and lattice parameter will strongly influence the ALD-CeO_2 growth. Therefore, to further improve the ALD-CeO_2 film quality on perovskite substrates, thorough studies of

dx.doi.org/10.1021/cm301864c | Chem. Mater. 2012, 24, 3732−3737

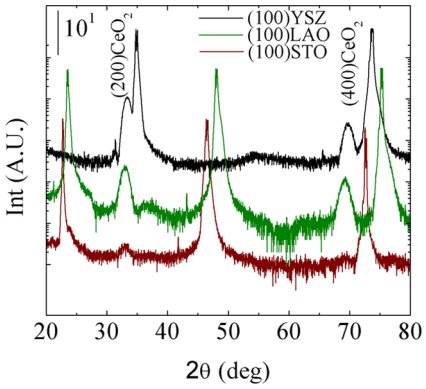

Figure 6. XRD θ–2θ scan of 400 cycles of ALD-CeO_2 on (100)YSZ, (100)LAO, and (100)STO single crystal substrates.

interfacial properties of each system are required. It is worth mentioning that the epitaxial growth of CeO_2 on STO and LAO reported using other deposition techniques as laser ablation or plasma-assisted molecular beam epitaxy was achieved at temperatures above 550 °C,[30,31] well above the temperatures used in this study.

Overall, it has been demonstrated that low temperature epitaxial ALD-CeO_2 films can be obtained on a wide number of substrates differing in crystal structure and lattice parameters which makes ALD a very attractive growth method for epitaxial oxides.

The reaction characteristics described above for ALD-CeO_2 make the preparation of nanosized features very challenging if SAMs or organic polymers are used as the resist layer, since they are removed during the oxidizing step in the ALD cycle. Here we have used Ag and PMMA and e-beam irradiation to overcome this issue (see Experimental Section). AFM images of the resulting nanostructres after the Ag etching are illustrated in Figure 7. Well-defined columnar and square-shaped features of

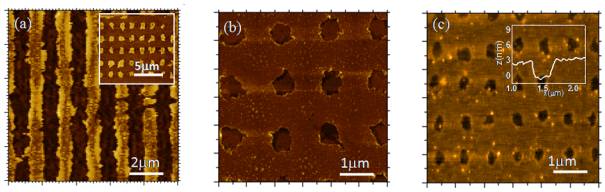

Figure 7. Atomic force microscopy of patterned 150 cycles ALD-CeO_2 films on YSZ substrate. (a) Linear motifs. Inset shows square-shaped CeO_2 nanostructures. (b and c) Nanohole array nanostructures. Inset shows the height profile of a nanohole from (c). Maximum height scale is 4 nm.

3 nm height and 600 nm width are observed in Figure 7a. Nanohole arrays can also be obtained with hole sizes ranging from 600 to 200 nm, Figure 7b,c, respectively. Thus, this is a very attractive approach to fabricate reproducible nanostructures with different sizes and shapes, which can be used as templates, even when metal precursor characteristics do not tolerate H_2O as oxidant for ALD deposition conditions.

CONCLUSIONS

In this work we demonstrate the preparation of highly epitaxial, ultrasmooth, and pure (001) CeO_2 ultrathin films down to 3 nm by atomic layer deposition (ALD) at a low deposition temperature, 275 °C, on single crystal substrates. ALD conditions have been optimized using cerium β-diketonate ($Ce(thd)_4$) and ozone (O_3) as precursors, resulting a growth per cycle of ≈0.2 Å/cycle. In contrast to conventional evaporation techniques, ALD offers low growth rates ensuring epitaxial film growth on crystalline substrates at low temperatures. Post-thermal treatments at 900 °C in oxygen further improve the ALD-CeO_2 film texture while maintaining film stoichiometry. Also, we demonstrate that combining e-beam lithography and ALD well-defined ALD-CeO_2 nanostructures can be easily obtained. Moreover, the versatility of this approach could easily be extended to a variety of oxides and substrates, opening many avenues for surface and interface engineering of functional oxides along with the study of interfacial properties.

ASSOCIATED CONTENT

Supporting Information

Thermal analysis of $Ce(thd)_4$ and detailed CeO_2 ALD growth characteristics. This material is available free of charge via the Internet at http://pubs.acs.org.

AUTHOR INFORMATION

Corresponding Author

*Phone: +34935801853. Fax: +34935805729. E-mail: mcoll@icmab.es.

Notes

The authors declare no competing financial interest.

ACKNOWLEDGMENTS

The authors would like to thank Dr. J. Bachmann of Hamburg University, Germany, for helpful discussions. This research was supported by MAT2011-28874-C02-01 and Consolider. M.C. acknowledges the JdC Spanish MICINN grant and J.G. acknowledges the JAE CSIC grant. Research performed in part at the Nanoquim facility within ICMAB-CSIC, Barcelona, Spain. We acknowledge the use of the X-ray photoelectron spectroscopy infrastructure available in the Laboratorio de Microscopías Avanzadas (LMA) at Instituto de Nanociencia de Aragón (University of Zaragoza, Spain) and the Scientific Services at ICMAB. Research at ORNL supported by the U.S. Department of Energy, Office of Basic Energy Science, Materials Sciences and Engineering Division. Instrument time provided by ORNL's Shared Research Equipment (ShaRE). User Facility supported by the U.S. Department of Energy, Office of Basic Energy Scince, Scientific User Facilities Division.

REFERENCES

(1) Campbell, C. T.; Peden, C. H. F. *Science* **2005**, *309* (5735), 713–714.
(2) Kilner, J. A. *Chem. Lett.* **2008**, *37* (10), 1012–1015.
(3) Trinchi, A.; Li, Y. X.; Wlodarski, W.; Kaciulis, S.; Pandolfi, L.; Viticoli, S.; Comini, E.; Sberveglieri, G. *Sens. Actuators, B* **2003**, *95* (1–3), 145–150.
(4) Tsunekawa, S.; Fukuda, T.; Kasuya, A. *J. Appl. Phys.* **2000**, *87* (3), 1318–1321.
(5) Kosynkin, V. D.; Arzgatkina, A. A.; Ivanov, E. N.; Chtoutsa, M. G.; Grabko, A. I.; Kardapolov, A. V.; Sysina, N. A. *J. Alloys Compd.* **2000**, 303421–425.
(6) http://www.itrs.net/ (2007).
(7) Sundaram, K. B.; Wahid, P. F.; Sisk, P. J. *Thin Solid Films* **1992**, *221* (1–2), 13–16.
(8) Norton, D. P.; Goyal, A.; Budai, J. D.; Christen, D. K.; Kroeger, D. M.; Specht, E. D.; He, Q.; Saffian, B.; Paranthaman, M.; Klabunde,

C. E.; Lee, D. F.; Sales, B. C.; List, F. A. *Science* **1996**, *274* (5288), 755−757.
(9) Pignolet, A.; Curran, C.; Alexe, M.; Senz, S.; Hesse, D. *Integr. Ferroelectr.* **1998**, *21* (1−4), 485−498.
(10) Kim, J. H.; Grishin, A. M.; Ignatova, V. A. *J. Electron. Mater.* **2008**, *37* (3), 361−367.
(11) Ami, T.; Ishida, Y.; Nagasawa, N.; Machida, A.; Suzuki, M. *Appl. Phys. Lett.* **2001**, *78* (10), 1361−1363.
(12) Trtik, V.; Aguiar, R.; Sanchez, F.; Ferrater, C.; Varela, M. *J. Cryst. Growth* **1998**, *192* (1−2), 175−184.
(13) Barreca, D.; Gasparotto, A.; Tondello, E.; Sada, C.; Polizzi, S.; Benedetti, A. *Chem. Vap. Deposition* **2003**, *9* (4), 199−206.
(14) Coll, M.; Gazquez, J.; Sandiumenge, F.; Puig, T.; Obradors, X.; Espinos, J. P.; Huhne, R. *Nanotechnology* **2008**, *19* (39), 395601.
(15) George, S. M. *Chem. Rev.* **2010**, *110* (1), 111−131.
(16) Parsons, G. N.; George, S. M.; Knez, M. *MRS Bull.* **2011**, *36* (November), 865−871.
(17) Ritala, M.; Kukli, K.; Rahtu, A.; Raisanen, P. I.; Leskela, M.; Sajavaara, T.; Keinonen, J. *Science* **2000**, *288* (5464), 319−321.
(18) Kim, D.; Kwon, J.-H.; Kim, M.; Hong, S.-H. *J. Cryst. Growth* **2011**, *322* (1), 33−37.
(19) Klepper, K. B.; Nilsen, O.; Fjellvag, H. *J. Cryst. Growth* **2007**, *307* (2), 457−465.
(20) Yum, J.; Bersuker, G.; Akyol, T.; Ferrer, D. A.; Lei, M. *IEEE Trans. Electron Devices* **2011**, *58* (12), 4384−4392.
(21) Bae, C.; Shin, H.; Nielsch, K. *MRS Bull.* **2011**, *36* (11), 887−897.
(22) Elam, J. W.; Dasgupta, N. P.; Prinz, F. B. *MRS Bull.* **2011**, *36* (11), 899−906.
(23) Jur, J. S.; Spagnola, J. C.; Lee, K.; Gong, B.; Peng, Q.; Parsons, G. N. *Langmuir* **2010**, *26* (11), 8239−8244.
(24) King, P. J.; Werner, M.; Chalker, P. R.; Jones, A. C.; Aspinall, H. C.; Basca, J.; Wrench, J. S.; Black, K.; Davies, H. O.; Heys, P. N. *Thin Solid Films* **2011**, *519* (13), 4192−4195.
(25) Paivasaari, J.; Putkonen, M.; Niinisto, L. *J. Mater. Chem.* **2002**, *12* (6), 1828−1832.
(26) Wrench, J. S.; Black, K.; Aspinall, H. C.; Jones, A. C.; Bacsa, J.; Chalker, P. R.; King, P. J.; Werner, M.; Davies, H. O.; Heys, P. N. *Chem. Vap. Deposition* **2009**, *15* (10−12), 259−261.
(27) Ohring, M. *Materials Science of Thin Films*, 2nd ed.; Academic Press: San Diego, 2002.
(28) Kim, Y. J.; Thevuthasan, S.; Shutthanandan, V.; Perkins, C. L.; McCready, D. E.; Herman, G. S.; Gao, Y.; Tran, T. T.; Chambers, S. A.; Peden, C. H. F. *J. Electron. Spectrosc.* **2002**, *126* (1−3), 177−190.
(29) Chen, L.; Chen, C. L.; Huang, D. X.; Lin, Y.; Chen, X.; Jacobson, A. J. *Solid State Ionics* **2004**, *175* (1−4), 103−106.
(30) Khodan, A. N.; Contour, J. P.; Michel, D.; Durand, O.; Lyonnet, R. *J. Cryst. Growth* **2000**, *209* (4), 828−841.
(31) Kim, Y. J.; Gao, Y.; Herman, G. S.; Thevuthasan, S.; Jiang, W.; McCready, D. E.; Chambers, S. A. *J. Vac. Sci. Technol. A* **1999**, *17* (3), 926−935.
(32) Conesa, J. C. *Surf. Sci.* **1995**, *339* (3), 337−352.
(33) Gibert, M.; Abellan, P.; Martinez, L.; Roman, E.; Crespi, A.; Sandiumenge, F.; Puig, T.; Obradors, X. *CrystEngComm* **2011**, *13* (22), 6719−6727.
(34) Gibert, M.; Puig, T.; Obradors, X.; Benedetti, A.; Sandiumenge, F.; Huhne, R. *Adv. Mater.* **2007**, *19* (22), 3937−+.
(35) Skorodumova, N. V.; Baudin, M.; Hermansson, K. *Phys. Rev. B* **2004**, *69* (7), 075401.
(36) Suzuki, M.; Ami, T. *Mater. Sci. Eng., B* **1996**, *41* (1), 166−173.
(37) Fors, R.; Khartsev, S. I.; Grishin, A. M. *Phys. Rev. B* **2005**, *71* (4), 045305.
(38) Coll, M.; Gazquez, J.; Huhne, R.; Holzapfel, B.; Morilla, Y.; Garcia-Lopez, J.; Pomar, A.; Sandiumenge, F.; Puig, T.; Obradors, X. *J. Mater. Res.* **2009**, *24* (4), 1446−1455.
(39) Wang, D. Y.; Kang, Y. J.; Doan-Nguyen, V.; Chen, J.; Kungas, R.; Wieder, N. L.; Bakhmutsky, K.; Gorte, R. J.; Murray, C. B. *Angew. Chem., Int. Ed.* **2011**, *50* (19), 4378−4381.
(40) Cui, M. Y.; He, J. X.; Lu, N. P.; Zheng, Y. Y.; Dong, W. J.; Tang, W. H.; Chen, B. Y.; Li, C. R. *Mater. Chem. Phys.* **2010**, *121* (1−2), 314−319.
(41) Ho, C. M.; Yu, J. C.; Kwong, T.; Mak, A. C.; Lai, S. Y. *Chem. Mater.* **2005**, *17* (17), 4514−4522.
(42) Jiang, X. R.; Bent, S. F. *J. Phys. Chem. C* **2009**, *113* (41), 17613−17625.
(43) Chen, R.; Kim, H.; McIntyre, P. C.; Bent, S. F. *Chem. Mater.* **2005**, *17* (3), 536−544.
(44) Ghosal, S.; Baumann, T. F.; King, J. S.; Kucheyev, S. O.; Wang, Y. M.; Worsley, M. A.; Biener, J.; Bent, S. F.; Hamza, A. V. *Chem. Mater.* **2009**, *21* (9), 1989−1992.
(45) Bachmann, J.; Zierold, R.; Chong, Y. T.; Hauert, R.; Sturm, C.; Schmidt-Grund, R.; Rheinlander, B.; Grundmann, M.; Gosele, U.; Nielsch, K. *Angew. Chem., Int. Ed.* **2008**, *47* (33), 6177−6179.
(46) Farm, E.; Kemell, M.; Ritala, M.; Leskela, M. *J. Phys. Chem. C* **2008**, *112* (40), 15791−15795.
(47) Ras, R. H. A.; Sahramo, E.; Malm, J.; Raula, J.; Karppinen, M. *J. Am. Chem. Soc.* **2008**, *130* (34), 11252−11253.
(48) McIntire, T. M.; Lea, A. S.; Gaspar, D. J.; Jaitly, N.; Dubowski, Y.; Li, Q. Q.; Finlayson-Pitts, B. J. *Phys. Chem. Chem. Phys.* **2005**, *7* (20), 3605−3609.
(49) Coll, M.; Richter, C. A.; Hacker, C. A. *J. Vac. Sci. Technol. B* **2009**, *27* (6), 2826−2831.
(50) Mackus, A. J. M.; Mulders, J. J. L.; van de Sanden, M. C. M.; Kessels, W. M. M. *J. Appl. Phys.* **2010**, *107* (11), 116102.
(51) Farm, E.; Lindroos, S.; Ritala, M.; Leskela, M. *Chem. Mater.* **2012**, *24* (2), 275−278.
(52) Becht, M.; Gerfin, T.; Dahmen, K. H. *Chem. Mater.* **1993**, *5* (1), 137−144.
(53) Abrutis, A.; Plausinaitiene, V.; Teiserskis, A.; Kubilius, V.; Senateur, J. P. *Chem. Vap. Deposition* **1999**, *5* (4), 171−177.
(54) Cavallaro, A.; Sandiumenge, F.; Gazquez, J.; Puig, T.; Obradors, X.; Arbiol, J.; Freyhardt, H. C. *Adv. Funct. Mater.* **2006**, *16* (10), 1363−1372.
(55) Paivasaari, J.; Niinisto, J.; Myllymaki, P.; Dezelah, C.; Winter, C. H.; Putkonen, M.; Nieminen, M.; Niinisto, L. In *Rare Earth Oxide Thin Films: Growth, Characterization, and Applications*; Fanciulli, M., Scarel, G., Eds.; Springer-Verlag: Berlin, 2007; Vol. *106*, pp 15−32.
(56) Tiitta, M.; Niinisto, L. *Chem. Vap. Deposition* **1997**, *3* (4), 167−182.
(57) Puurunen, R. L. *Chem. Vap. Deposition* **2003**, *9* (5), 249−257.
(58) Elliott, S. D. *Semicond. Sci. Technol.* **2012**, *27* (7), 074008.
(59) Puurunen, R. L. *Chem. Vap. Deposition* **2003**, *9* (6), 327−332.
(60) Coll, M.; Gazquez, J.; Pomar, A.; Puig, T.; Sandiumenge, F.; Obradors, X. *Phys. Rev. B* **2006**, *73* (7), 075420.
(61) Paparazzo, E.; Ingo, G. M.; Zacchetti, N. *J. Vac. Sci. Technol. A* **1991**, *9* (3), 1416−1420.
(62) Wagner, C. D.; Naumkin, A. V.; Kraut-Vass, A.; Allison, J. W.; Powell, C. J.; Rumble, J. R. J. 2000.
(63) Lewis, B. *Thin Solid Films* **1971**, *7* (3−4), 179−&.
(64) Krug, J.; Politi, P.; Michely, T. *Phys. Rev. B* **2000**, *61* (20), 14037−14046.
(65) Chvoj, Z.; Tringides, M. C.; Chromcova, Z. *J Phys.: Condens. Matter* **2011**, *23* (21), 215307.
(66) Zhao, P.; Ito, A.; Tu, R.; Goto, T. *Surf. Coat. Technol.* **2011**, *205* (16), 4079−4082.
(67) Nandasiri, M. I.; Nachimuthu, P.; Varga, T.; Shutthanandan, V.; Jiang, W. *J. Appl. Phys.* **2011**, *109* (1), 013525.
(68) Solovyov, V. F.; Develos-Bagarinao, K.; Nykypanchuk, D. *Phys. Rev. B* **2009**, *80* (10), 104102.
(69) Cavallaro, A.; Burriel, M.; Roqueta, J.; Apostolidis, A.; Bernardi, A.; Tarancon, A.; Srinivasan, R.; Cook, S. N.; Fraser, H. L.; Kilner, J. A.; McComb, D. W.; Santiso, J. *Solid State Ionics* **2010**, *181* (13−14), 592−601.
(70) Garcia-Barriocanal, J.; Rivera-Calzada, A.; Varela, M.; Sefrioui, Z.; Iborra, E.; Leon, C.; Pennycook, S. J.; Santamaria, J. *Science* **2008**, *321* (5889), 676−680.